

# Effect of mechanical milling on the structural, magnetic and dielectric properties of coprecipitated ultrafine zinc ferrite

S.D. Shenoy<sup>a</sup>, P.A. Joy<sup>b</sup>, M.R. Anantharaman<sup>a,\*</sup>

<sup>a</sup>Department of Physics, Cochin University of Science and Technology, Thrikkakara, Cochin 682 022, India

<sup>b</sup>Physical Chemistry Division, National Chemical Laboratory, Pune 411 008, India

Received 15 March 2003; received in revised form 23 June 2003

## Abstract

Nanosized  $\text{ZnFe}_2\text{O}_4$  particles containing traces of  $\alpha\text{-Fe}_2\text{O}_3$  by intent were produced by low temperature chemical coprecipitation methods. These particles were subjected to high-energy ball milling. These were then characterised using X-ray diffraction, magnetisation and dielectric studies. The effect of milling on zinc ferrite particles have been studied with a view to ascertaining the anomalous behaviour of these materials in the nanoregime. X-ray diffraction and magnetisation studies carried out show that these particles are associated with strains and it is the surface effects that contribute to the magnetisation. Hematite percentage, probably due to decomposition of zinc ferrite, increases with milling. Dielectric behaviour of these particles is due to interfacial polarisation as proposed by Koops. Also the defects caused by the milling produce traps in the surface layer contributes to dielectric permittivity via spin polarised electron tunnelling between grains. The ionic mechanism is enhanced in dielectrics with the rise in temperature which results in the increase of dielectric permittivity with temperature.

© 2003 Published by Elsevier B.V.

PACS: 75.50.K; 75.50.G; 75.30.P; 77.22.E; 81.20.W

Keywords: Magnetic nanoparticles; Zinc ferrite; High-energy ball milling; Superparamagnetism; Spinel; Strain parameter; Dielectric; Interfacial polarisation; Spin polarised tunnelling; Lab VIEW

## 1. Introduction

Nanoparticles have been generating extensive interest in recent years among researchers worldwide owing to their interesting physical and chemical properties with respect to their coarser sized cousins in the bulk [1–5]. Nanoparticles of many ferrites have been successfully obtained by

numerous chemical routes, such as reverse micelle synthesis, coprecipitation, thermal decomposition, solgel and aerogel process [1–12]. High-energy ball milling (HEBM) is being extensively employed as an alternate route to obtain novel materials through solid state reactions [5,6,13–21].

Ferrites are ferrimagnetic materials containing iron oxide as the main constituent with various metal oxides. They have been extensively studied both for understanding these systems from a theoretical point of view and in deriving newer materials based on ferrites for possible applications.

\*Corresponding author. Tel.: +91-484-2577404; fax: +91-484-2577595.

E-mail address: [mra@cusat.ac.in](mailto:mra@cusat.ac.in) (M.R. Anantharaman).

Ferrites and materials derived from ferrites find extensive application in devices like transformers, TV yokes, loud speakers and in a horde of other devices. They are also one of the largely used material medium for audio/video applications and computer memories [6,12]. They have the general formula  $\{(M)_\delta(Fe)_{1-\delta}\}[(M)_{1-\delta}(Fe)_{1+\delta}]O_4$ . The divalent metal ion M (e.g. Zn, Mg, Mn, Fe, Co, Ni or a mixture of them) can occupy either tetrahedral (*A*) or octahedral (*B*) sites as depicted by curled and square brackets, respectively [1,3–10,22,23]. In the above formula when  $\delta = 1$ , it is called normal spinel and when  $\delta = 0$ , it is called inverse spinel. When  $\delta = 1/3$ , it is called a random spinel.  $C = 1 - \delta$  represents the inversion parameter.

In the coarser regime, the magnetic and structural properties of these ferrites are determined by a variety of factors like Madelung energy, cationic size, charge and site preference energy. For example cation like  $Ni^{2+}$  and  $Zn^{2+}$  have exclusive octahedral and tetrahedral site preferences, respectively [2–5,7,8,10,12,24]. So in a typical Nickel ferrite, Nickel occupies only the octahedral (*B*) sites and this results in an inverse spinel while in zinc ferrite, zinc occupies tetrahedral (*A*) sites exclusively and results in a normal spinel.

There are numerous reports where in anomaly in structural and magnetic properties of these ferrites in the ultrafine regime have been reported. For instance, zinc ferrite which is purported to be a normal spinel, is a classic example of an antiferromagnetic material with a Neel temperature of 10 K. Ultrafine  $ZnFe_2O_4$  have been reported to be exhibiting a net magnetic moment at room temperature [1,3,5–10,14,22,25,26]. From the application point of view, zinc ferrites are widely used catalysts [5] and in the nano regime, the modification of surface properties will have a profound bearing in determining the catalytic properties of these materials. Moreover, since they exhibit useful magnetisation at room temperature in the nano regime they can be potential materials for other applications too.

Zinc ferrite if prepared in the nanoregime, exhibits inversion and the percentage of occupancy of  $Zn^{2+}$  ion depends on the method of prepara-

tion, vis-à-vis cold preparation technique or ball milling etc [1,3,4,7,8,15]. Results by Hamdeh et al [1,3,8] show a relatively high inversion parameter when coprecipitation methods are employed. There are also reports indicating that ball milling facilitates inversion and induces magnetic ordering [3,8,15]. In inverse spinels like nickel ferrite, redistribution from inverse to mixed spinel type occurs at nanolevel resulting in an enhancement in magnetisation as compared to the bulk. Chinnasamy et al. [22,24] reported an 8% increase in the value of  $M_s$  for 1 h milled nickel ferrite. But prolonged milling reduced the  $M_s$  value because of spin-glass like surface disorder exhibited by the particles in the ultrafine regime. The theoretical and technological lowest size of magnetically ordered systems are still an open question of major relevance to applications of nano structured systems in high density magnetic recording devices [6]. So research on fine particle zinc ferrite is of utmost interest in understanding the behavior at the nanolevel.

Preliminary studies carried out by Anantharaman et al. [10] on ultrafine zinc ferrite by employing techniques like Low energy ion scattering, Mössbauer spectroscopy and Vibration sample magnetometry revealed that in the nano regime, zinc ferrite exhibits an altogether different magnetic structure with a net magnetisation at room temperature. From the theoretical point of view the origin of magnetism in systems similar to ultrafine  $ZnFe_2O_4$  is an important question, which is under debate now, and still no conclusive theory has been formulated. The relevance of dead layer theory also is to be examined on systems belonging to the family of inverse spinels like nickel ferrite in the nano regime where a dead layer formation in the surface have been invoked to account for the reduced magnetisation exhibited by the fine particles. This aspect and the unusual behaviour of  $ZnFe_2O_4$  nanoparticles coupled with the unusual claim of zinc ions occupying a substantial number of octahedral sites motivated this work [11]. It has also been reported that zinc ferrite decomposes to  $\alpha-Fe_2O_3$  and magnetic  $ZnFe_2O_4$  during continued milling. That was on particles prepared by ceramic technique and subjected to HEBM subsequently. In the present study

ZnFe<sub>2</sub>O<sub>4</sub> is synthesized by coprecipitation methods with traces of  $\alpha$ -Fe<sub>2</sub>O<sub>3</sub> and these are subjected to HEBM.

The dielectric properties of nano particle ferrite materials are influenced mainly by the method of preparation, cation distribution, grain size, sintering temperature, oxygen parameter, the ratio of Fe<sup>2+</sup>/Fe<sup>3+</sup> ions and oxygen anion vacancies in lattices [27]. So far, there exists no convincing reports on dielectric properties of nano particle ferrites which throws light on the conduction mechanism of these materials in the ultrafine regime.

The effect of ball milling on the structural, magnetic and dielectric properties of the fine particles is investigated. This is intended to check the claim by various researchers that ZnFe<sub>2</sub>O<sub>4</sub> shows anomalous behaviour when prepared in the nanoregime by employing coprecipitation methods. Moreover, this is a sequel to our investigations on fine particle normal spinel ferrites.

## 2. Experimental

### 2.1. Preparation of ZnFe<sub>2</sub>O<sub>4</sub> by coprecipitation

Zinc ferrite was prepared by low temperature preparative techniques as described by Sato et al [9,28]. Aqueous solution of zinc nitrate of 0.1 m and ferric nitrate of 0.2 m were prepared separately. Thousand millilitres of each solution was mixed together. While stirring the mixture, 25% ammonia solution was added until pH attains 11 at 373 K. The precipitate was dried at 373 K and annealed in air at 573 K which yielded zinc ferrite [10]. This sample is labelled as ZFP.

### 2.2. Mechanical treatment using HEBM

The milling of original ZnFe<sub>2</sub>O<sub>4</sub> prepared as above was carried out in a closed container using a planetary ball mill (Fritsch pulverisette 7). A portion of the powder was placed in a tungsten carbide vial with 8:1 ball to powder weight ratio keeping milling intensity at 360 rpm. Tungsten carbide balls and toluene as liquid carrier was employed for HEBM. Powders were milled at two

different milling times—30 and 300 min. The samples were labelled as ZF30 and ZF300, respectively.

### 2.3. Structural studies

The structural studies on these samples were carried out using the method of X-ray powder diffraction. The powder diffractogram was recorded on a Rigaku *D*-MaxC model X-ray diffractometer using Cu K $\alpha$  radiation ( $\lambda = 1.5418 \text{ \AA}$ ) in the  $2\theta$  range 10–80° with a step size of 0.05° and a speed of 2°/min. The lattice constants of the spinel compounds were estimated from the X-ray diffraction peak positions. The average crystallite size *D* was obtained by employing Scherrer's formula from the line broadening of the XRD peak corresponding to the (3 1 1) plane of the spinel structure and also by strain calculations. The phases present were identified by comparing the peak positions and intensities with those listed in the JCPDS file.

### 2.4. Magnetisation studies

The room temperature and low temperature (liquid nitrogen) magnetic characterization were carried out using a vibrating sample magnetometer (Model:EG&G PAR 4500). Magnetization curves at 300 K and 83 K were recorded for ZFP, ZF30 and ZF300. Saturation magnetisation ( $M_s$ ) and Coercivity ( $H_c$ ) were obtained from these measurements.

### 2.5. Dielectric studies

The dielectric studies were carried out using a homebuilt dielectric cell and an HP 4285A impedance analyser in the frequency range 100 KHz to 10 MHz. The details of the set up are cited elsewhere [27]. The temperature could be varied from room temperature to 393 K by a digital temperature controller. Samples in the form of pellets were employed for the evaluation of dielectric permittivity ( $\epsilon_r$ ). If *c* is the capacitance of the sample, *d* its thickness and *A* the surface area, then,  $\epsilon_r = cd/\epsilon_0 A$  where  $\epsilon_0$  is the dielectric constant of the air. All the measurements were

carried out under high vacuum. The impedance analyser was interfaced via a GPIB card to a PC and the data acquisition was completely automated by employing the LabVIEW software (National Instruments).

### 3. Results and discussion

#### 3.1. Structural

XRD pattern of the samples is shown in the Fig. 1. XRD pattern indicates the presence of small amounts of  $\alpha$ -Fe<sub>2</sub>O<sub>3</sub> in all the three samples whose percentage first decreases and then increases with milling time.

Fig. 2 shows the relative intensities ( $I/I_0 \times 100$ ) of (121), (231) and (211) planes which are the three strongest lines of  $\alpha$ -Fe<sub>2</sub>O<sub>3</sub> with respect to the intensity of most prominent (311) plane of ZnFe<sub>2</sub>O<sub>4</sub>. During the initial stage of milling, some unreacted ferric and zinc salts and the  $\alpha$ -Fe<sub>2</sub>O<sub>3</sub> present may react to form ZnFe<sub>2</sub>O<sub>4</sub> and thereby  $\alpha$ -Fe<sub>2</sub>O<sub>3</sub> line gets less intense during the first 30 min of milling. But during prolonged milling, due to nanometer sized grains, high local pressures and temperatures during collisions with balls and vial, and the subsequent kinetic energy produced will lead to a decomposition of ZnFe<sub>2</sub>O<sub>4</sub> in the milling process [13,21,29]. There are reports of production of Fe<sub>3</sub>O<sub>4</sub> (by product of  $\alpha$ -Fe<sub>2</sub>O<sub>3</sub>) as a result of

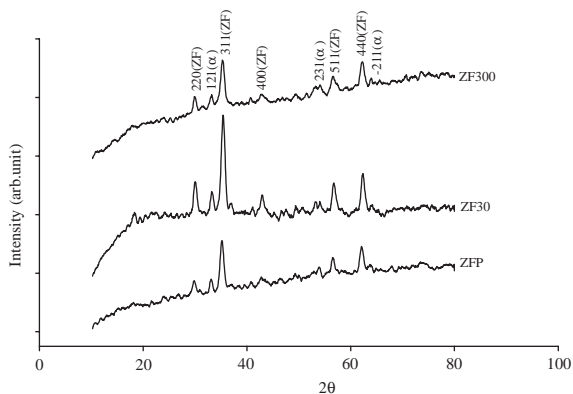


Fig. 1. XRD pattern of ZFP ZF30 ZF300 showing  $\alpha$ -Fe<sub>2</sub>O<sub>3</sub>( $\alpha$ ) impurity lines and ZnFe<sub>2</sub>O<sub>4</sub>(ZF) lines.

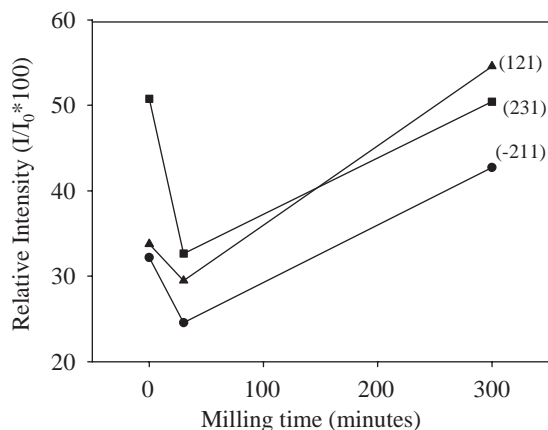


Fig. 2. Intensity variation of prominent  $\alpha$ -Fe<sub>2</sub>O<sub>3</sub> lines with milling time.

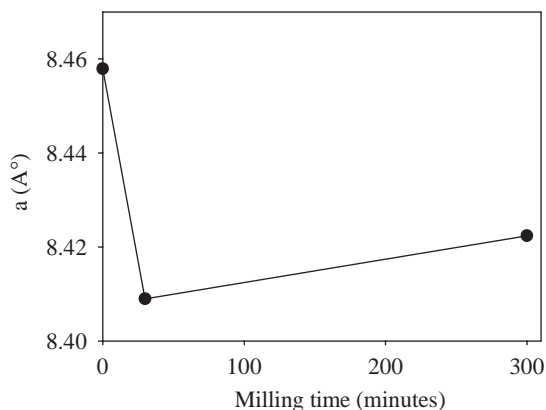


Fig. 3. Lattice parameter variation with milling time.

prolonged milling [30]. But in our present study no traces of Fe<sub>3</sub>O<sub>4</sub> were detected by XRD.

Lattice parameter of coprecipitated unmilled sample is found to be 8.46 Å which is higher than the standard value reported in JCPDS of 8.44 Å (Fig. 3). This is in agreement with the results obtained by other researchers [3,8,9,13]. Lattice parameter is found to be decreasing with milling. The probable reason for this lattice parameter reduction may be the inversion of cations taking place with milling. There are also reports suggesting that as inversion increases lattice parameter decreases [28]. Since Zn<sup>2+</sup> has a large ionic radius than Fe<sup>3+</sup>, this site reversal will cause a decrease

of lattice constant [29]. This effect has not been observed in sintered (ceramic) ferrite. The other probable reason for this unique property of coprecipitated sample may be the presence of lattice defects and its influence on ultrafine particles, especially on the surface. In ultrafine particles surface energy and surface tension of particles are high. This results in a tendency to shrink the lattice which causes reduced lattice constant [28]. It is also possible that the cation distributions do differ between those present near the particle's surface and those of non-surface atoms. This situation is highly probable for the materials with a large number of defects in which  $O^{2-}$  ions are missing from normally occupied sites and/or in which  $Fe^{3+}$  occupies normally unoccupied sites. In such instances, however, it is clear that the crystal chemical structure is not those appropriate to spinel ferrites [11]. This disordered structure can also be attributed to the strong internal strains introduced during mechanical treatment [4,31,32].

It is known that the inversion if any, in these systems can be detected by analysing the intensities ratios of 220/400 lines. The intensity ratio corresponding to these planes have been calculated. If the samples produced have an inverse component in it (i.e. that is the reversal of cations) then 220/400 lines must show a decreasing intensity ratio from that of normal one. For normal spinels the intensity ratio should be 35/17. Our result is in agreement with cation distributions corresponding to the normal spinel and also exhibits no change with milling. So inversion, if any, cannot be deduced from the XRD results. However XRD is not an advisable tool to deal with cation occupancy, hence neutron scattering is recommended.

Size of the particle decreases as the milling time increases because the kinetic energy generated by the series of collisions among balls is transferred to the system [33] but there is no sudden decrease as in the case of ceramic powders (Fig. 4). This is because the starting powder (coprecipitated) itself is of nanometer sized. Also there are reports that within 24 min of milling, size reduction may attain its maximum [13]. The other reason for not obtaining a great reduction in size is due to the high local temperature and pressure generated

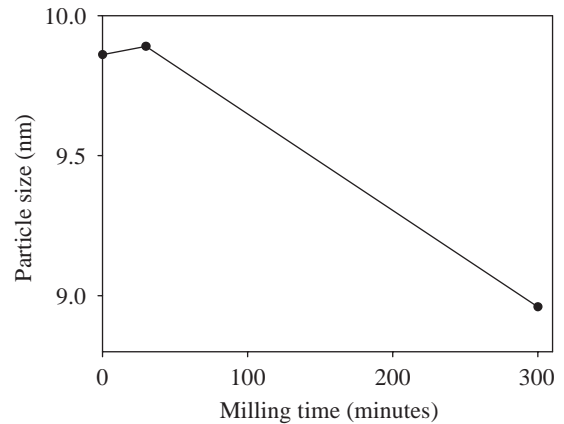


Fig. 4. Particle size reduction with milling.

during the combustion as a result of the high-energy ball milling [34].

The grain size and the strain developed during the milling process can be calculated from the linewidth (FWHM in radian) of XRD lines as follows [35]:

$$\text{FWHM}(\beta) = \lambda/(d_g \cos \theta) + 4\varepsilon \tan \theta, \quad (1)$$

where  $\theta$  is the bragg angle,  $\varepsilon$  is the strain developed and  $d_g$  the grain size.

Rewriting the above equation

$$\beta \cos \theta = \varepsilon(4 \sin \theta) + \lambda/d_g. \quad (2)$$

This equation represents a straight line between  $\beta \cos \theta$  (Y-axis) and  $4 \sin \theta$  (X-axis). The slope of this line gives the strain and  $d_g$  can be calculated from the intercept of this line on the Y-axis. The particle size when calculated by employing Scherrer's formula at different  $\theta$  values was at variance. This is an indication of the presence of strain.

Fig. 5 shows  $4 \sin \theta$  vs.  $\beta \cos \theta$  lines for ZFP, ZF30 and ZF300. The grain sizes calculated from this graphs almost match with the one calculated by Scherer formula for the most intense line.

Strain values are also calculated and found to be increasing with milling time and are plotted in Fig. 6. Strain continues to increase with an increase in the milling time.

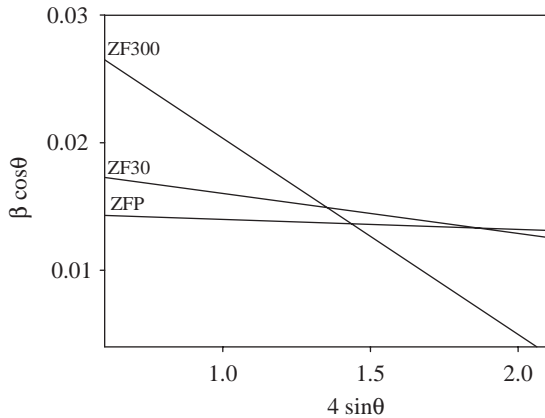


Fig. 5.  $4 \sin \theta - \beta \cos \theta$  graphs indicating the presence of strain.

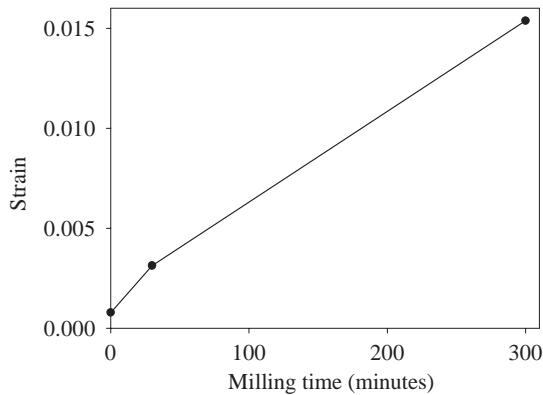


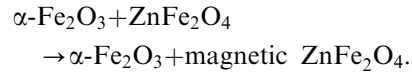
Fig. 6. Milling time dependence on the strain which increases with milling time.

### 3.2. Magnetisation

Fig. 7 shows typical results for magnetisation curves taken at 300 K and 83 K for ZFP, ZF30, ZF300, respectively. Room temperature curves show typical superparamagnetic behaviour with no hysteresis. That is, both retentivity and coercivity are zero, which is in tune with the results obtained by other researchers [9,29,36–38].

Fig. 8 depicts the variation of saturation magnetisation with milling time. The strain associated with fine particles, as a result of milling, produces a disorder by displacement of ions, which is one cause for an increase in magnetisation. In ultrafine particles large fractions of atoms are located on the surface and therefore the surface

effects, which include surface energy and surface tension as well as the change in position of anions and cations, will favour an increase of magnetisation, although hematite percentage may increase. Furthermore, hematite may be acting as a facilitator in producing magnetic zinc ferrite, which is magnetic due to the strain and surface effects. This can be written in the following form:



From Fig. 6 it is evident that the strain increases tetra fold for ZF300 with respect to ZF30. But from Fig. 8, one does not observe a corresponding increase in magnetisation for 300 min milled sample. Though strain produces disorder and thereby contributes to overall magnetisation (could be because of surface spins) there is another possibility. Since we are seeing  $M_s$  in emu/gm, the overall increase in magnetisation may be masked by the increased amount of  $\alpha\text{-Fe}_2\text{O}_3$  which increases with milling as evidenced by XRD.

The hysteresis behaviour completely vanishes at room temperature. Short-range magnetic ordering of Fe spins at 83 K contributes to magnetic hysteresis loops. Long range ordering is expected at liquid helium temperature. These powders exhibit a net magnetisation and are magnetically ordered at much higher temperature than that of normal zinc ferrite. It may be noted here that for mechanically milled sample,  $T_N$  has been reported to be  $\sim 115$  K [14]. The magnetic ordering starts with the formation of superparamagnetic clusters whose size gradually increases with lowering temperature, superparamagnetic clusters present are heterogeneous at room temperature but get ordered at lower temperature to contribute to magnetisation [1].

Superparamagnetic relaxation time  $\tau$ , which is the average time required for the particle to jump from one axis of magnetisation to another is given by the relation

$$\tau = \tau_0 \exp(K_{\text{eff}} V / k_B T_B), \quad (3)$$

where  $k_B T_B$  is the thermal energy,  $K_{\text{eff}}$  is the effective anisotropy constant and  $V$  the particle volume.  $\tau$  increases with decreasing temperature resulting in an enhanced magnetisation. Also

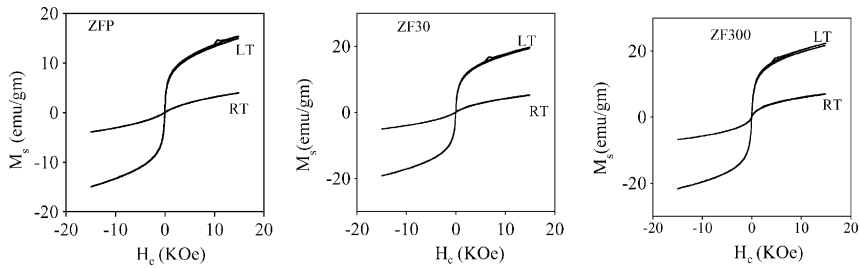


Fig. 7. Magnetisation curves of ZFP ZF30 ZF300 at K(RT) and 83 K (LT).

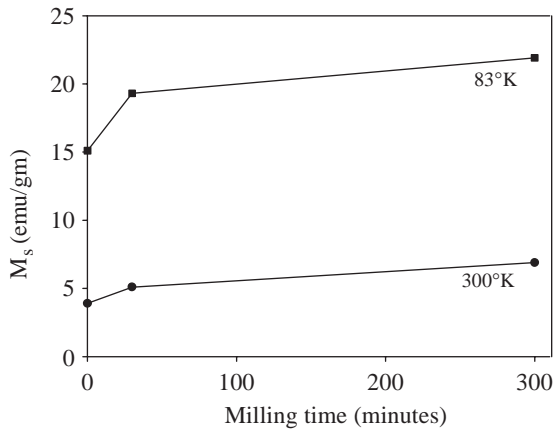


Fig. 8. Dependence of milling time on saturation magnetisation.

the saturation magnetisation ( $M_s$ ) is governed by the following equation [39]:

$$M_s = \frac{2K}{H_c} \left[ 1 - (25kT/KV)^{1/2} \right]. \quad (4)$$

According to the above relation  $M_s$  increases with decrease of temperature and this is in agreement with our results.

Coprecipitation results in large structural and chemical disorder. Ball milling will produce greater atomic disorder due to mechanical displacement of ions under high stress and shear. This order may contribute to magnetisation [1,6,8].

As the particle size (hence the volume) decreases the probability of thermally activated magnetisation increases. Surface effects become increasingly important as the particle volume decreases. So surface effects could not be ruled out in the fine particle systems [40–42].

As the inversion increases, the material makes the transition to ferromagnetism through complex magnetic states [1]. One complex state is the distribution of  $\text{Fe}^{3+}$  and  $\text{Fe}^{2+}$  ions and the oxygen vacancies resulting from milling which can create the super exchange paths and induce spin disorder [14]. Cation distribution may also differ between those present near the particle's surface and those of non-surface atoms [11,43]. This FM ordering coupled with the antiferromagnetically (AFM) ordered  $\alpha\text{-Fe}_2\text{O}_3$  may produce FM–AFM exchange interaction that can modify magnetic properties as suggested by various researchers [18–19]. But the dispersion of FM clusters in an AFM matrix is ruled out here since  $\alpha\text{-Fe}_2\text{O}_3$  percentage is small [21].

### 3.3. Dielectric

The dielectric properties of ferrites are influenced by various factors out of which the grain size plays a key role. The samples which assumed heterogeneous nature due to the individual grains influences the dielectric variation with frequency. Thus the dielectric behaviour of the ferrites is attributed primarily to interfacial polarisation resulting from their heterogeneous structure comprising low resistivity grains separated by high resistivity grain boundaries as suggested by Koops phenomenological dispersion theory [44–47]. The  $\text{Fe}^{2+}$  and  $\text{Fe}^{3+}$  ions present in ferrites contribute effectively to produce interfacial polarisation. This is supported by the inverse proportionality between dielectric permittivity and resistivity as observed by various researchers.

Fig. 9 shows the dielectric variation with frequency. The oxygen ion vacancies produced

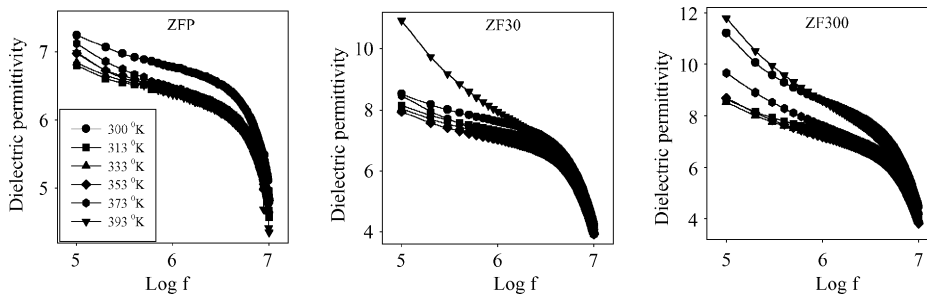


Fig. 9. Variation of dielectric permittivity with log (frequency) different temperatures.

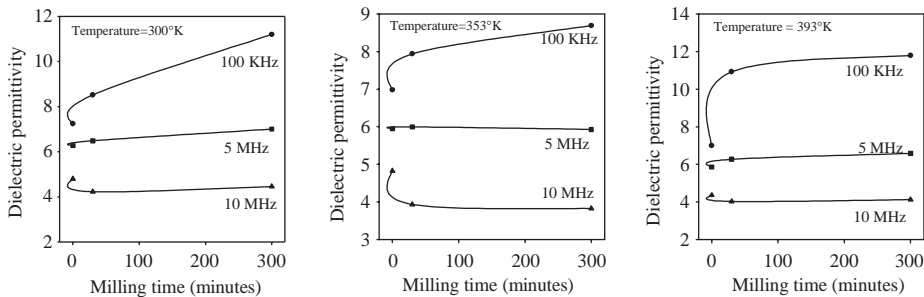


Fig. 10. Variation of dielectric constant with milling time at different frequencies (at fixed temperatures).

during ball milling may also contribute to dielectric permittivity which is predominant at lower frequencies [48]. The non-uniformity of the structure increases with reduction in size according to our XRD results. Hence this should increase the dielectric permittivity of ball milled samples and our results are in accordance with this (Fig. 10).

The traps formed at the grain boundaries are not of uniform shape and may become the cause for deviation from parallel alignment of moments of individual grains. Electrons are then transferred from one grain to another by a process called spin polarised tunnelling in which electron spin is conserved. Tunnelling probability of spin polarised electrons is larger when the magnetisation of the particles is aligned [43]. This will increase the dielectric permittivity with milling.

Fig. 10 clearly shows the enhancement of dielectric permittivity at low frequencies. However, dielectric permittivity decreases at higher frequencies since the mobility of charge carriers is low at higher frequencies and cannot follow the alternation of applied AC electric field [49].

The temperature dependence of dielectric permittivity at different frequencies is shown in Fig. 11. In dielectrics, the ionic mechanism of polarisation increases dielectric permittivity when the temperature increases. When the temperature rises, the orientation of dipoles gets facilitated resulting in an increased permittivity. But at very high temperatures the chaotic thermal oscillations of molecules are intensified and the degree of orderliness of their orientation is diminished, thus the permittivity passes through a maximum value. We observe that the variation of dielectric permittivity with temperature at low frequencies (100 KHz) is much more pronounced than at higher frequencies.

#### 4. Conclusions

XRD results indicate that the particles formed are ultrafine and associated with strains. The structural and magnetic studies on the milled  $\text{ZnFe}_2\text{O}_4$  samples indicate that zinc ferrite in the

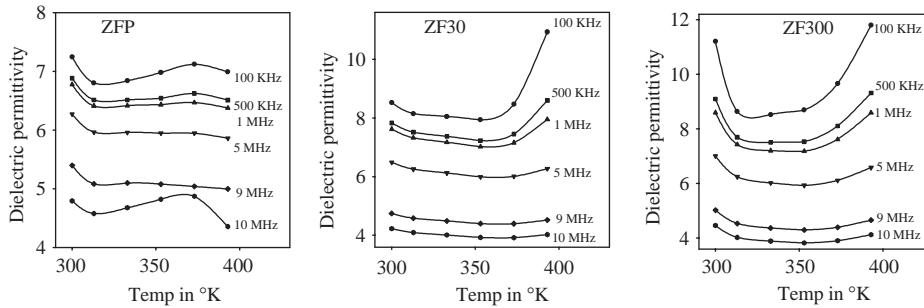


Fig. 11. Variation of dielectric permittivity with temperature (at different frequencies).

ultrafine regime exhibit net magnetisation. Strain increases with milling producing an atomic disorder due to displacement of the position of both anions and cations. Particle size measured show that they are around 10 nm and no much decrease with milling. This is because of the nanosized starting precursor and the high local temperature produced while milling. The prolonged milling does not increase magnetisation much appreciably, which may be due to the fact that the overall increase in magnetisation may be masked by the increased amount of  $\alpha$ - $\text{Fe}_2\text{O}_3$ , which increases with milling. Dielectric behaviour of these particles is due to interfacial polarisation as proposed by Koops. The  $\text{Fe}^{2+}$  ions produced causes  $\text{Fe}^{2+} \rightleftharpoons \text{Fe}^{3+}$  hopping and the oxygen ion vacancy in the lattice contribute to dielectric permittivity. The ionic mechanism is enhanced in dielectrics with the rise in temperature, which results in the increase of permittivity with temperature. A clear understanding of this anomalous behaviour of zinc ferrite in the nano regime warrants further studies using neutron scattering and/or ESCA.

### Acknowledgements

One of the authors, MRA thanks Third World Academy of Sciences (TWAS), Trieste, Italy for financial assistance received through project (Ref. No. 00-118/RG/PHYS/AS). SDS and MRA thank Inter University Consortium for Department of Atomic Energy Facilities (IUC-DAEF), Govt. of India for financial support through project (Ref. No. IUC/MUM/CRS-M-60).

### References

- [1] J.C. Ho, H.H. Hamdeh, Y.S. Chen, S.H. Lin, Y.D. Yao, R.J. Willey, S.A. Oliver, *Phys. Rev. B* 52 (1995) 10122.
- [2] W.C. Kim, S.J. Kim, Y.R. Uhm, C.S. Kim, *IEEE Trans. Magn.* 37 (2001) 2362.
- [3] H.H. Hamdeh, J.C. Ho, S.A. Oliver, R.J. Willey, G. Oliveri, G. Busca, *J. Appl. Phys.* 81 (1997) 1851.
- [4] B. Jeyadevan, K. Tohji, K. Nakatsuka, *J. Appl. Phys.* 76 (1994) 6325.
- [5] H. Ehrhardt, S.J. Campbell, M. Hofmann, *J. Alloys Compounds* 339 (2002) 255.
- [6] G.F. Goya, H.R. Richenberg, M. Chen, W.B. Yelon, *J. Appl. Phys.* 87 (2000) 8005.
- [7] T. Kamiyama, K. Haneda, T. Sato, S. Ikeda, H. Asano, *Sol. State Commun.* 81 (1992) 563.
- [8] H.H. Hamdeh, J.C. Ho, S.A. Oliver, R.J. Willey, J. Kramer, Y.Y. Chen, S.H. Lin, Y.D. Yao, M. Daturi, G. Busca, *IEEE Trans. Magn.* 31 (1995) 3808.
- [9] T. Sato, K. Haneda, M. Seki, T. Iijima, *Appl. Phys. A* 50 (1990) 13.
- [10] M.R. Anantharaman, S. Jagatheesan, K.A. Malini, S. Sindhu, A. Narayanasamy, C.N. Chinnasamy, J.P. Jacobs, S. Reijne, K. Seshan, R.H.H. Smits, H.H. Brongersma, *J. Magn. Magn. Mater.* 189 (1998) 83.
- [11] M.T. Clerk, B.J. Evans, *IEEE Trans. Magn.* 33 (1997) 3745.
- [12] T. Pannaparayil, S. Komarneni, R. Marande, M. Zadarko, *J. Appl. Phys.* 67 (1990) 5509.
- [13] V. Sepelak, K. Tkacova, V.V. Boldyrev, S. Wibmann, K.D. Becker, *Physica B* 234–236 (1997) 617.
- [14] G.F. Goya, H.R. Rechenberg, *J. Magn. Magn. Mater.* 196–197 (1999) 191.
- [15] V. Sepelak, P. Druska, U. Sleinike, *Mater. Struct.* 6 (1999) 100.
- [16] B.S. Murty, S. Ranganathan, *Int. Mater. Rev.* 43 (1998) 101.
- [17] K. Haneda, H. Kojima, *J. Am. Ceram. Soc.* 57 (1974) 68.
- [18] J. Sort, J. Nogues, X. Amils, S. Surinach, J.S. Munoz, M.D. Baro, *Appl. Phys. Lett.* 75 (1999) 3177.

- [19] J. Sort, J. Nogues, S. Surinach, J.S. Munoz, M.D. Baro, E. Chappel, F. Dupont, G. Chouteau, Appl. Phys. Lett. 79 (2001) 1142.
- [20] Z. Jin, W. Tang, J. Zhang, H. Lin, Y. Du, J. Magn. Magn. Mater. 182 (1998) 231.
- [21] W.A. Kaczmarek, B. Idzikowski, K.H. Muller, J. Magn. Magn. Mater. 177–181 (1998) 921.
- [22] C.N. Chinnasamy, A. Narayanasamy, N. Ponpandian, K. Chattopadhyay, K. Shinoda, B. Jeyadevan, K. Tohji, K. Nakatsuka, T. Furubayashi, I. Nakatani, Phys. Rev. B63 (2001) 184108.
- [23] J.M. Hastings, L.M. Corliss, Phys. Rev. 102 (1956) 1460.
- [24] C.N. Chinnasamy, A. Narayanasamy, N. Ponpandian, R.J. Justin, B. Jeyadevan, K. Tohji, K. Chattopadhyay, J. Magn. Magn. Mater. 238 (2002) 281.
- [25] W. Schiessel, W. Potzel, H. Karzel, M. Steiner, G.M. Kalvius, A. Martin, M.K. Krause, I. Halevy, J. Gal, W. Schafer, G. Will, M. Hillberg, R. Wappling, Phys. Rev. B 53 (1996) 9143.
- [26] F.K. Lotgering, J. Phys. Chem. Solids 27 (1996) 139.
- [27] E.M. Mohammed, K.A. Malini, P. Kurian, M.R. Anantharaman, Mater. Res. Bull. 37 (2002) 753.
- [28] T. Sato, IEEE Trans. Magn. Magn. 6 (1970) 795.
- [29] Q. Chen, A.J. Rondinone, B.C. Chakoumakos, J.Z. Zhang, J. Magn. Magn. Mater. 194 (1999) 1.
- [30] G.F. Goya, H.R. Rechenberg, J.Z. Jiang, J. Appl. Phys. 84 (1998) 1101.
- [31] D. Arcos, R. Valenzuela, M. Vazquez, M. ValletRegi, J. Solid State Chem. 141 (1998) 10.
- [32] M.I. Rosales, O.A. Valenzuela, R. Valenzuela, IEEE Trans. Magn. 37 (2001) 2373.
- [33] C. Suryanarayana, G.H. Chen, F.H. Samfroes, Scr. Metall. 26 (1992) 1727.
- [34] J. Ding, T. Tsuzuki, P.G. McCormick, R. Street, J. Magn. Magn. Mater. 162 (1996) 271.
- [35] S. Manojkumar, S. Sekhon, J. Phys. D 34 (2001) 2995.
- [36] M. Zheng, X.C. Wu, B.S. Zou, Y.J. Wang, J. Magn. Magn. Mater. 183 (1998) 152.
- [37] V. Masheva, M. Grigorova, N. Valkov, H.J. Blythe, T. Midlarz, V. Blaskov, J. Geshev, M. Mikhov, J. Magn. Magn. Mater. 196–197 (1999) 128.
- [38] Q. Chen, J.Z. Zhang, Appl. Phys. Lett. 73 (1998) 3156.
- [39] B.D. Cullity, Introduction to Magnetic Materials. Addison-Wesley, London, 1972, p. 415.
- [40] R.V. Upadhyay, Pramana 49 (1997) 309.
- [41] K. Haneda, Can. J. Phys. 65 (1987) 1233.
- [42] A.H. Morrish, K. Haneda, X.Z. Zhou, Proceedings of the NATO Advanced Study Institute on Nanophase Materials-Syntheses, Properties and Applications, Kluwer Academic, Netherlands, 1994, p. 515.
- [43] X. Battle, A. Laborta, J. Phys. D 35 (2002) R15.
- [44] C.G. Koops, Phys. Rev. 83 (1951) 121.
- [45] D. Ravinder, A.V.R. Reddy, G. Rangamohan, Mater. Lett. 52 (2002) 259.
- [46] V.P. Miroshkin, Y.A.I. Panova, V.V. Passynkov, Phys. Stat. Sol. (A) 66 (1981) 179.
- [47] V.R.K. Murthy, B. Viswanathan, Ferrite Materials Science and Technology, Narosa Publishing House, New Delhi, 1990, 15, 60.
- [48] N. Ponpandian, A. Narayanasamy, J. Appl. Phys. 92 (5) (2002) 2770.
- [49] A.M. Abdeen, J. Magn. Magn. Mater. 192 (1999) 121.